

## ORIGINAL ARTICLE

NOMA-GAP/*ARHGAP33* regulates synapse development and autistic-like behavior in the mouseS Schuster<sup>1</sup>, M Rivalan<sup>2</sup>, U Strauss<sup>3</sup>, L Stoenica<sup>3</sup>, T Trimbuch<sup>4</sup>, N Rademacher<sup>5</sup>, S Parthasarathy<sup>6</sup>, D Lajkó<sup>1,6</sup>, C Rosenmund<sup>4</sup>, SA Shoichet<sup>5</sup>, Y Winter<sup>2</sup>, V Tarabykin<sup>6</sup> and M Rosário<sup>1</sup>

Neuropsychiatric developmental disorders, such as autism spectrum disorders (ASDs) and schizophrenia, are typically characterized by alterations in social behavior and have been linked to aberrant dendritic spine and synapse development. Here we show, using genetically engineered mice, that the Cdc42 GTPase-activating multiadaptor protein, NOMA-GAP, regulates autism-like social behavior in the mouse, as well as dendritic spine and synapse development. Surprisingly, we were unable to restore spine morphology or autism-associated social behavior in NOMA-GAP-deficient animals by Cre-mediated deletion of Cdc42 alone. Spine morphology can be restored *in vivo* by re-expression of wild-type NOMA-GAP or a mutant of NOMA-GAP that lacks the RhoGAP domain, suggesting that other signaling functions are involved. Indeed, we show that NOMA-GAP directly interacts with several MAGUK (membrane-associated guanylate kinase) proteins, and that this modulates NOMA-GAP activity toward Cdc42. Moreover, we demonstrate that NOMA-GAP is a major regulator of PSD-95 in the neocortex. Loss of NOMA-GAP leads to strong upregulation of serine 295 phosphorylation of PSD-95 and moreover to its subcellular mislocalization. This is associated with marked loss of surface  $\alpha$ -amino-3-hydroxy-5-methyl-4-isoxazolepropionic acid (AMPA) receptor and defective synaptic transmission, thereby providing a molecular basis for autism-like social behavior in the absence of NOMA-GAP.

*Molecular Psychiatry* (2015) **20**, 1120–1131; doi:10.1038/mp.2015.42; published online 14 April 2015

## INTRODUCTION

Defective formation and maturation of dendrites and dendritic structures is associated with a myriad of neurodevelopmental disorders, ranging from intellectual disability to neuropsychiatric disorders such as schizophrenia and autism spectrum disorders (ASDs). Alterations in both the degree of branching of the dendritic tree and in the maturation of dendritic spines in cortical neurons have been described in these conditions. The molecular reasons for these changes, however, remain largely elusive.

Neuropsychiatric developmental disorders have been described as diseases of the synapse (reviewed in Penzes *et al.*<sup>1</sup>). The MAGUK (membrane-associated guanylate kinase) family of proteins, which include DLG1/SAP97, DLG2/PSD-93, DLG3/SAP102, DLG4/PSD-95, CASK and MAGI, are important PDZ-containing scaffold proteins that are involved in recruiting receptors, such as the glutamate receptors and various other signaling and adaptor molecules involved in synaptic transmission, to the synapse. As such, they have important roles in synapse development and function and are involved in long-term potentiation and depression, as well as in the development of neurological and psychiatric disease.<sup>2</sup> Gene variation and deletion of *DLG3/SAP102*, for instance, is associated with intellectual disability in humans.<sup>3,4</sup> In addition, many of the candidate molecules so far identified for ASD and schizophrenia are directly or indirectly associated and regulated by PSD-95 and/or regulate PSD-95 function. These include the PSD-95-associated Shank scaffold proteins<sup>5,6</sup> and Neuroligin adhesion molecules,<sup>7</sup> as well as the disease-associated kinases CDKL5 (ref. 8) and

JNK3.<sup>9</sup> Although mutations in PSD-95 itself have so far not been identified in ASD patients, PSD-95-deficient mice show increased repetitive behavior and anxiety, as well as aberrant social interactions.<sup>10</sup>

Rho family GTPases are cytoskeletal regulators whose de-regulation is associated with the intellectual disability and potentially also with neuropsychiatric disorders (reviewed in Govek *et al.*<sup>11</sup>, Bennett<sup>12</sup> and Tolia *et al.*<sup>13</sup>). These proteins, which include Rho, Rac and Cdc42, cycle between active GTP and inactive GDP-bound states. Cycling is regulated by association with a number of guanine nucleotide exchange factors, guanine nucleotide dissociation inhibitors and GTPase-activating proteins (GAPs).<sup>11</sup>

Previously, we described a novel neuronal GAP, called NOMA-GAP (gene name *ARHGAP33*), which is specific for the Rho family member Cdc42. We showed that NOMA-GAP is the major negative regulator of Cdc42 during development of the mammalian neocortex, where it is required for induction of complex dendritic branching patterning.<sup>14</sup>

We now present evidence that NOMA-GAP/*ARHGAP33* regulates autism-like behavior, as well as the maturation of dendritic spines and synaptic function in mice. In the neocortex, the Cdc42-GAP activity of NOMA-GAP, is sufficient to direct dendritic complexity, but is not required for dendritic spine morphology, synaptic function, or for NOMA-GAP-dependent aspects of autism-associated social behavior. However, we show that NOMA-GAP directly interacts with several MAGUK family proteins, colocalizing with PSD-95 at dendritic spines heads. Furthermore, NOMA-GAP

<sup>1</sup>Dendritic Development, Institute of Cell and Neurobiology, Charité Universitätsmedizin Berlin, Berlin, Germany; <sup>2</sup>Institute of Cognitive Neurobiology, Humboldt University Berlin and Berlin Mouse Clinic for Neurology and Psychiatry, Charité Universitätsmedizin, Berlin, Germany; <sup>3</sup>Ionic Current Development, Institute of Cell and Neurobiology, Charité Universitätsmedizin Berlin, Berlin, Germany; <sup>4</sup>Neuroscience, NeuroCure—NWFZ, Charité Universitätsmedizin Berlin, Berlin, Germany; <sup>5</sup>Molecular Neurobiology and Genetics, NeuroCure—NWFZ, Charité Universitätsmedizin Berlin, Berlin, Germany and <sup>6</sup>Cortical Development, Institute of Cell and Neurobiology, Charité Universitätsmedizin Berlin, Berlin, Germany. Correspondence: Dr M Rosário, Dendritic Development, Institute of Cell and Neurobiology, Charité Universitätsmedizin Berlin, Charitéplatz 1, Berlin 10117, Germany. E-mail: marta.rosario@charite.de

Received 6 April 2014; revised 23 February 2015; accepted 3 March 2015; published online 14 April 2015

regulates PSD-95 function by directing the subcellular localization and phosphorylation of PSD-95. In addition, this interaction negatively regulates the Cdc42-GAP activity of NOMA-GAP, indicating a two-way regulation. We propose that the interaction of NOMA-GAP with PSD-95 generates a delicate balance in the regulation of Cdc42 and PSD-95 that permits correct spine maturation and synaptic transmission. NOMA-GAP is thus also a promising candidate for neuropsychiatric pathophysiology.

## MATERIALS AND METHODS

### Reagents

A detailed list of reagents including plasmid constructs used is provided in Supplementary Information.

### Mice

All mouse experiments were carried out according to German law and approved by the Landesamt für Gesundheit und Soziales Berlin. NOMA-GAP-deficient and Cdc42 floxed cre mice are all C57Bl/6 background and were described previously.<sup>14</sup> Nex1-Cre transgenic animals are C57Bl/6 background and have been described previously.<sup>15</sup>

*In utero* electroporations were carried out at E15.5 as described previously.<sup>14</sup> Electroporated brains were prepared 23 days after birth (P23), fixed in 4% paraformaldehyde/phosphate-buffered saline (PBS) and sectioned at 50  $\mu$ m using a vibratome (Leica VT1200, Leica Microsystems, Wetzlar, Germany).

### Behavioral testing

Male and female littermate mice were tested in a battery of behavioral tests from 6 to 7 months of age on and in the following order: (i) general

health check based on SHIRPA protocol, (ii) control of the sensory functions using the visual cliff test and (iii) the buried food test, (iv) evaluation of species specific abilities during burrowing test, (v) marble burying test and (vi) nest construction test, (vii) screening of natural behaviors in home cage and (viii) in open field, (ix) evaluation of social preference and recognition in the three-chamber apparatus and (x) in the partition test. Limb clasp was evaluated at 4 time points across the 18 weeks of testing. Male control, N<sup>-/-</sup> and N<sup>-/-</sup> Cdc42 fl/+ Cre littermate 3-month-old mice were tested in a smaller battery of behavioral tests. After regular health check, the mice were tested in the three-chamber test and their behaviors were screened in the home cage. This phase of testing lasted 7 weeks including breaks between tests. For details on behavioral tests and statistical analysis, see Supplementary Information.

### Cell culture, transfection and infection

HEK 293 cells were grown in Dulbecco's modified Eagle's medium (Gibco, Life Technologies, Carlsbad, CA, USA) supplemented with 10% fetal calf serum (FCS; Biochrom, Merck KGaA, Darmstadt, Germany) and antibiotics (Gibco). Transfections were carried out using Lipofectamine 2000 (Life Technologies, Carlsbad, CA, USA) according to the manufacturer's instructions.

Primary cortical neurons were prepared from littermate E16.5 embryos and grown at 37 °C in 5% CO<sub>2</sub> in neurobasal medium (Gibco) supplemented with 1% B27 (Gibco), 1x Glutamax (Gibco), 25  $\mu$ M  $\beta$ -mercaptoethanol and 1x penicillin/streptomycin (Gibco) as described previously.<sup>14</sup> Cultured neurons were transfected using Effectene Transfection Reagent (Qiagen, Hilden, Germany) according to the manufacturer's protocol. N<sup>+/-</sup> and N<sup>+/+</sup> neurons are used as controls. N<sup>+/-</sup> and N<sup>+/+</sup> animals are indistinguishable in terms of the behavior tested, cortical development and dendritic morphology (Figures 1b and c, Figures 3a and b).<sup>14</sup>

Overexpression of NOMA-GAP in mature primary cortical cultures was achieved by lentiviral infection. Primary cortical neuron cultures were

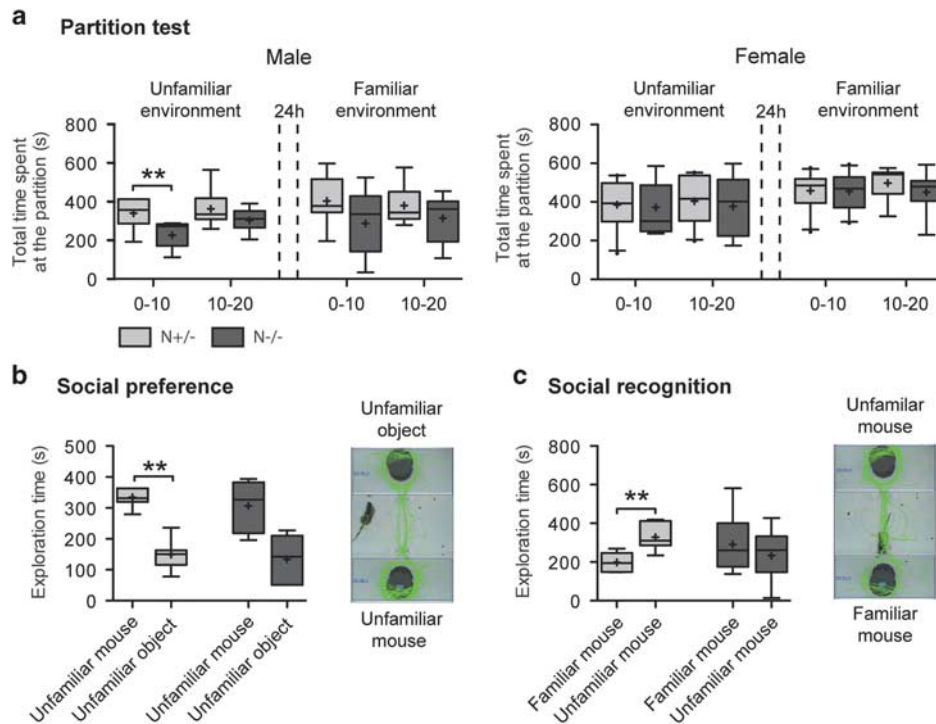


**Figure 1.** NOMA-GAP regulates social behavior in the mouse. **(a)** Reduced interaction of NOMA-GAP-deficient mice with unfamiliar mice in a partitioned chamber. The time spent (s) by NOMA-GAP-deficient mice at a partition separating test and unfamiliar mouse was determined per bins of 10 min. ( $n = 7$  male, 10 female control and 7 male, 7 female N<sup>-/-</sup> mice). In the unfamiliar environment condition, the home cage is new to the test mouse. For the familiar environment test, the test mouse spent 24 h in the partitioned chamber in the absence of other mice. Unfamiliar environment, Mann-Whitney *U*-test for two independent samples  $U = 5$ ,  $**P < 0.01$ . **(b)** NOMA-GAP-deficient male mice show reduced social preference. Mice were tested in a three-chambered apparatus containing an unfamiliar mouse in one side-chamber and an empty container (unfamiliar object) in the other. ( $n = 7$  male mice for each genotype;  $**P < 0.01$ ). Time spent in each chamber was determined. **(c)** Loss of NOMA-GAP is associated with impaired social recognition in male mice. The time spent by the test mouse in each side-chamber of a three-chambered apparatus containing a familiar mouse in one side-chamber and an unfamiliar mouse in the other was determined. ( $n = 7$  male mice for each genotype; non-parametric Wilcoxon signed ranks test for paired samples,  $P < 0.01$ ).

infected with 10  $\mu$ l of the viral solution ( $0.5\text{--}1 \times 10^6$  IU ml<sup>-1</sup>) at 7 days *in vitro* (DIV 7) and analyzed at DIV 20. Please see Supplementary Information for details on viral production.

Biotinylation of surface proteins was carried out on DIV 20 primary cortical neurons. Cells were washed in rinsing solution (PBS pH 7.5 containing 0.1 mM CaCl<sub>2</sub> and 1 mM MgCl<sub>2</sub>) and labeled for 30 min at 4 °C in rinsing solution containing 1 mg ml<sup>-1</sup> Sulfo-NHS-SS-Biotin (Pierce Protein Research Products, Life Technologies, Carlsbad, CA, USA). The reaction was quenched using rinsing solution containing 100 mM glycine followed by washing in rinsing solution.

### Immunoprecipitation and western blotting

Protein concentrations were determined using the BCA Protein Assay Kit (Pierce Protein Research Products). Lysates used for the precipitation of biotinylated proteins and for the co-immunoprecipitation of endogenous proteins from the neocortex of adult mice were prepared in RIPA buffer (50 mM Tris, 150 mM NaCl, 1% vol/vol NP-40, 0.1% wt/vol sodium dodecyl sulfate, 0.5% wt/vol deoxycholate, pH 7.4) containing inhibitors (1x Protease inhibitor cocktail (Calbiochem, Merck KGaA, Darmstadt, Germany), 1x PhosStop (Roche, Basel, Switzerland), 1 mM Na<sub>3</sub>VO<sub>4</sub>, (Sigma-Aldrich, St. Louis, MO, USA)) and clarified by centrifugation at 13 500 r.p.m. at 4 °C for 15 min. Biotinylated proteins were precipitated using avidin agarose beads (Pierce Protein Research Products) for 1 h at 4 °C. Co-immunoprecipitation of endogenous proteins were carried out with the indicated antibodies and protein G sepharose beads for 3 h at 4 °C. All precipitates were washed thoroughly in Tris-buffered saline buffer (50 mM Tris pH 7.4, 100 mM NaCl), and finally boiled in sample buffer for 5 min.

For analysis of protein:protein interactions, transfected HEK 293 cells were harvested 24 h after transfection, lysed in FLAG buffer (50 mM Tris pH 7.5, 100 mM NaCl, 1 mM EDTA, 1% v/v Triton X100) containing inhibitors (1x Protease inhibitor cocktail (Sigma-Aldrich), 1 mM Na<sub>3</sub>VO<sub>4</sub>, 10  $\mu$ g ml<sup>-1</sup> leupeptin, 1 mM benzamide, 5  $\mu$ g ml<sup>-1</sup> pepstatin, 1x PhosStop (Roche)) and cleared by 20 min centrifugation at 14 000 r.p.m. 4 °C. Tagged proteins were immunoprecipitated using anti-Myc 9B11 (Cell Signaling Technology, Danvers, MA, USA) or anti-green fluorescent protein (GFP; Rockland Immunochemicals, Limerick, PA, USA) antibodies for 3 h at 4 °C and then captured on protein G Sepharose beads (GE Healthcare Europe, Freiburg, Germany). Beads were washed thoroughly before boiling in sample buffer.

Stimulations of HEK 293 cells were carried out with 100 ng ml<sup>-1</sup> epidermal growth factor for 10 min before lysis in RIPA buffer as before.

Sodium dodecyl sulfate–polyacrylamide gel electrophoresis separation of proteins was carried out with equal amounts of protein. Separated proteins were transferred to Immobilon-P Transfer membranes (Millipore, Merck KGaA, Darmstadt, Germany) and detected by incubation with the indicated antibodies followed by incubation with appropriate peroxidase-coupled secondary antibodies (Jackson ImmunoResearch Laboratories, Pike West Grove, PA, USA). Visualization was achieved by chemiluminescence (ECL Western Blotting Detection Reagents; PerkinElmer, Waltham, MA, USA). Chemiluminescence was captured and quantified using the Image Lab Software on a ChemiDoc XRS+ detector (Bio-Rad Laboratories, Hercules, CA, USA).

### Immunofluorescence

Immunofluorescent staining was carried out as described previously.<sup>14</sup> Briefly, samples were stained in parallel after permeabilization and blocking as follows: HEK 293 cells were incubated in 0.1% TX100/PBS for 20 min followed by 10% FCS/PBS for 30 min, cultured cortical neurons in 0.1% TX100, 5% FCS, 1% bovine serum albumin (BSA; Serva Electrophoresis, Heidelberg, Germany) in PBS for 30 min, and brain sections in 0.2% TX100, 10% FCS, 1% BSA in PBS for 1 h.

All primary antibody incubations were carried out overnight at 4 °C. Antibodies were diluted in either 10% FCS/Tris-NaCl-blocking buffer (0.1 M Tris HCl 150 mM NaCl, pH 7.5) for HEK cells, 5% FCS, 1% BSA/PBS for cortical neurons or in 0.1% TX100, 5% FCS, 1% BSA in PBS for tissue sections. Following washing, samples were then incubated with appropriate fluorochrome-coupled secondary antibody (Jackson ImmunoResearch Laboratories) for 2 h at room temperature. Labeling of surface GluR1 was carried out in non-permeabilized cells, after blocking with 5% FCS, 1% BSA/PBS for 30 min, by incubation with primary antibody overnight at 4 °C in PBS. Cells were then washed and permeabilized and blocked as described above for 30 min and incubated with the appropriate fluorochrome-coupled secondary antibody and phalloidin-TRITC (Sigma-Aldrich).

All fluorescent images were captured on a confocal Leica SL using the same settings across compared samples.

Please see Supplementary Information for further details on the morphometric analysis of dendritic spines.

### Electrophysiology

Slices of mouse brains (21–28 days old) were used for *ex vivo* recordings. After brief anesthesia with isoflurane, mice were decapitated, brains removed and transferred to ice-cold artificial cerebrospinal fluid containing 85 mM NaCl, 26 mM NaHCO<sub>3</sub>, 2.5 mM KCl, 1 mM NaH<sub>2</sub>PO<sub>4</sub>, 0.5 mM CaCl<sub>2</sub>, 7 mM MgCl<sub>2</sub>, 50 mM sucrose and 10 mM glucose. Coronal slices (400  $\mu$ m nominal thickness) containing the somatosensory cortex were cut on a Leica VT1200 (Leica Microsystems, Wetzlar, Germany). Slices were allowed to recover for 30 min at 34 °C and kept at room temperature afterward.

Somatic whole-cell recordings were performed in a submerged recording chamber perfused with artificial cerebrospinal fluid containing 117 mM NaCl, 3.5 mM KCl, 1.25 mM NaH<sub>2</sub>PO<sub>4</sub>, 2 mM MgSO<sub>4</sub> or MgCl<sub>2</sub>, 2 mM NaHCO<sub>3</sub>, 10 mM glucose and 2 mM CaCl<sub>2</sub>. Pyramidal neurons were identified in the upper layers (L2/3) of somatosensory cortex using an upright microscope equipped with infrared differential interference contrast optics (Axioskop FS2; Zeiss, Oberkochen, Germany or Olympus BX51, Olympus Europe, Hamburg, Germany) and approached with patch pipettes (tip resistance 3–5 M $\Omega$ ) filled with intracellular solution containing 120 mM K-gluconate, 10 mM KCl, 10 mM Na-phosphocreatine, 1 mM MgCl<sub>2</sub>, 1 mM CaCl<sub>2</sub>, 11 mM EGTA, 10 mM HEPES, 2 mM Mg<sup>2+</sup>-ATP, 0.3 mM Tris-GTP, (pH 7.25, 288 mOsm). Only neurons with resting potentials below –65 mV and spiking characteristics of principal neurons were considered. There was no difference in either neuronal size or series resistance between the groups (Supplementary Figure S6).

Postsynaptic currents were recorded in continuous voltage clamp at a holding potential of –60 mV. Miniature excitatory postsynaptic currents were isolated with 1  $\mu$ M TTX (Tocris, Bristol, UK) and 10  $\mu$ M bicuculline. All artificial cerebrospinal fluid solutions were constantly perfused with 95% O<sub>2</sub>/5% CO<sub>2</sub>, osmolarity was maintained in the range of 290–305 mosmol l<sup>-1</sup> and all experiments were performed at 32–34 °C.

Data from patch-clamp recordings were collected with an EPC-10 double amplifier (HEKA Elektronik Dr. Schulze, Lambrecht/Pfalz, Germany), digitized (6.25 kHz, after Bessel filtering at 2.9 kHz) and stored using PatchMaster software (HEKA). Series resistance (R<sub>s</sub>) was monitored throughout experiments; cells were rejected if R<sub>s</sub> was >20 M $\Omega$  or varied >  $\pm$  30% during the recording. No R<sub>s</sub> compensation was used. Liquid junction potentials (~10 mV) were not corrected for.

Events were detected offline using Mini Analysis Program (Synaptosoft Inc., Fort Lee, NJ, USA) using a threshold of 2.5 times noise standard deviation of regions without manually detectable postsynaptic currents. All events were counterchecked by eye.

### Statistics

Statistical significance was calculated as indicated in the figure legends. Please see Supplementary Information for full descriptive statistical information on the data presented (Supplementary Table S2) and for additional information on statistical analysis of the behavioral data. Briefly, statistics were performed using Origin7 (OriginLab Corporation, Northampton, MA, USA) or GraphPad Prism for Mac OS X, Version 5.0A (GraphPad Software, La Jolla, CA, USA). For normal distributed data sets (Shapiro–Wilk test) the two tailed Student's *t*-tests was used. In the case of significant deviations from normal distribution ( $P \leq 0.05$ ), the non-parametric Mann–Whitney *U*-test was used. Graphs show averages  $\pm$  s.e. m. unless otherwise stated and probability outcomes are summarized in the graphs as following: NS, not significant, \* $P < 0.05$ , \*\* $P < 0.01$  and \*\*\* $P < 0.001$ .

## RESULTS

### NOMA-GAP regulates social behavior in mice

Previously, we generated a mouse model with a loss-of-function mutation in the *ARHGAP33* gene (encoding the protein NOMA-GAP) and showed that these mice have a thinner neocortex associated with defective dendritic branching of cortical neurons during development.<sup>14</sup> We now addressed the effect of this mutation on animal health and behavior using a battery of standardized tests. General screening revealed no gross alterations in

animal health, sensory perception or in general patterns of behavior (Supplementary Table S1 and Figures S1–S2). However, we observed increased hindlimb clasping in NOMA-GAP-deficient (N<sup>-/-</sup>) male animals (Supplementary Figure S1D), a phenotype commonly observed in mouse models for various neurological disorders including ASD and related disorders.<sup>16</sup>

Explorative behavior, tested in the novel environment of an open field was unaltered in terms of the level of general mouse activity or time spent in the center/periphery of the field (Supplementary Figures S3A and C). In multiple tests, however, we saw indications for increased anxiety in NOMA-GAP-deficient mice. Namely, in the new environment of the open field, male NOMA-GAP-deficient mice showed increased number of freezing bouts and female NOMA-GAP-deficient mice showed a tendency for increased number of freezing and grooming bouts (Supplementary Figures S3E and F). Female NOMA-GAP-deficient mice also showed increased latency to enter the center of the field (Supplementary Figure S3D). In addition, NOMA-GAP-deficient mice built more complex nests and buried the first foreign object (marbles) faster than control animals in nest-building (Supplementary Figures 4A and D) and burrowing tests (Supplementary Figure S4E), respectively. Increased number of freezing bouts, increased grooming in novel environment, increased nest complexity and faster burying of foreign objects may represent increased levels of anxiety or perceived stress in NOMA-GAP-deficient mice.

Next, we assessed social behavior in tests designed for the characterization of autism-like behavior in mice.<sup>17,18</sup> First, the interest of the test mouse for an unfamiliar mouse was evaluated in a cage where the two mice were separated by a clear and pierced wall (Figure 1a). Control and NOMA-GAP-deficient female mice showed a similar preference for exploring the unfamiliar mouse. However, we found that male NOMA-GAP-deficient mice spent less time in the partition zone compared with control animals at the start of the test when the cage was new to the test mouse. This suggests that when there is a conflict between exploration of the novel environment and of the novel mouse, NOMA-GAP-deficient mice have a reduced preference for the novel mouse. After familiarization with the environment, NOMA-GAP-deficient male mice still exhibited a decreased tendency to approach the partition separating it from an unfamiliar mouse (Figure 1a).

Male mice were then tested in a three-chamber arena, where the central compartment is connected to two compartments on either side, one of which contained an unfamiliar mouse in a small wire cage and the other an empty wire cage.<sup>17,19</sup> Control mice showed a clear significant preference for exploring the compartment containing the unfamiliar mouse. This preference, however, was absent in NOMA-GAP-deficient male mice (Figure 1b). There was no significant difference in the latency to enter the chamber containing the stranger mouse between control and mutant mice (control 57.59 s s.d. 49.7; N<sup>-/-</sup> 110.7 s s.d. 62.4; Mann-Whitney *U*-test). The comparable behavior of control and NOMA-GAP-deficient mice in the novel environment of the open field test (Supplementary Figures 3A and C), in sensory and motoric tests (Supplementary Figures S1A and C and in general health and activity (Supplementary Table S1 and Supplementary Figure S2), suggests that the alterations in social preference shown by NOMA-GAP-deficient male mice are not due to differences in exploratory behavior or to limitations in physical or sensory functions.

Following this social preference test, we assessed social recognition by testing the mouse's ability to distinguish between a familiar mouse and a new unfamiliar one. As has been previously described, control mice show a clear preference for a compartment containing the unfamiliar mouse. Remarkably, NOMA-GAP-deficient mice, failed to discriminate between the familiar and unfamiliar mouse (Figure 1c).

These data indicate that NOMA-GAP-deficient male mice have marked deficits in social behavior that are reminiscent of typical autistic traits in humans.

#### NOMA-GAP regulates dendritic spine maturation and synaptic transmission

ASDs are characterized by alterations in dendritic spine development in humans.<sup>20</sup> NOMA-GAP has previously been detected in the postsynaptic fraction of adult mouse brain lysates.<sup>21</sup> We analyzed the subcellular location of NOMA-GAP more closely. A GFP-tagged NOMA-GAP fusion protein was expressed together with a DsRed expression construct in upper layer cortical neurons in the mouse brain (Figure 2a). The electroporation control, DsRed, was observed in both dendrites and in axons of upper layer neurons. NOMA-GAP, however, was only detectable in dendrites and was absent from axons. We also expressed Myc and GFP-tagged-NOMA-GAP in mature (DIV 20) cultured primary cortical neurons (Figures 2b and c) and observed concentration of NOMA-GAP at the heads of dendritic spines, as well as along the dendritic shaft. Indeed, NOMA-GAP colocalized with the postsynaptic protein PSD-95 at dendritic spine head, although interestingly we saw no colocalization in the dendritic shaft (Figure 2c).

Next, we addressed whether NOMA-GAP regulates dendritic spine development by quantifying density and morphological features of dendritic spines along basal dendrites in upper layer cortical neurons of adult NOMA-GAP-deficient mice (Figure 2d). *In utero* electroporation of a GFP expression construct into the cortex of E15.5 embryos was used to facilitate visualization of dendritic morphology at 23 days post-partum (P23). Loss of NOMA-GAP was associated with an increase in the length of dendritic spine necks in layer 2/3 neurons (Figure 2e) but no change in spine head width was detected (Figure 2f). We also observed an increase in spine density (Figure 2g). We observed similar alterations in spine morphology in cultured NOMA-GAP-deficient primary cortical neurons (Supplementary Figures S5A and D). Increased spine neck length is thought to indicate spine immaturity and correlates inversely with synaptic efficacy.<sup>22,23</sup> This defect, together with increased spine density, comprises the most obvious alterations in the cortex of ASD patients.<sup>1</sup>

As morphological changes may result in aberrant synaptic transmission, we recorded spontaneous postsynaptic currents (sPSC) of upper layer cortical neurons in brain slices from adult NOMA-GAP-deficient and wild-type littermate animals (Figure 2h). Despite increased spine density, we found a pronounced drop in sPSC frequency (Figure 2i) in neurons from NOMA-GAP-deficient animals ( $9.3 \pm 0.9 \text{ s}^{-1}$ ) when compared with those of wild-type littermates ( $24.8 \pm 2.0 \text{ s}^{-1}$ ) but no alteration in amplitude (Figure 2j) or waveform (sPSC decay to 37%:  $5.0 \pm 0.4 \text{ ms}$ ,  $n = 23$  vs  $4.8 \pm 0.3 \text{ ms}$ ,  $n = 20$ ,  $P = 0.7$ , respectively). Notably, the frequency drop in NOMA-GAP-deficient neurons occurred despite an increase in input resistance upon loss of NOMA-GAP (Supplementary Figure S6B), suggesting an underestimation of the actual effect.

At a holding potential of  $-60 \text{ mV}$ , sPSCs were inward and short lived and therefore consistent with the activation of  $\alpha$ -amino-3-hydroxy-5-methyl-4-isoxazolepropionic acid receptors (AMPA). In line with this, direct comparison of spontaneous vs miniature excitatory postsynaptic currents in the same neurons (Supplementary Figure S6D) suggests that, as previously found,<sup>24</sup> most if not all spontaneous events in upper layer neurons in cortical slices around resting potential are miniature, excitatory, most likely AMPA-mediated, postsynaptic currents (mEPSCs) rather than inhibitory or presynaptic action potential-driven, regardless of the NOMA-GAP content.

Changes in mEPSC frequency are interpreted as either resulting from altered probability of presynaptic vesicle release at existing

synapses or from changes in the number of functional synapses.<sup>25</sup> Given that NOMA-GAP is specifically located at the postsynaptic site, we addressed whether NOMA-GAP regulates the number of excitatory synapses, identified by the opposing expression of the

presynaptic marker synaptophysin and the postsynaptic protein PSD-95 (Figures 2k and l). Figure 2l shows that loss of NOMA-GAP results in a significant decrease in the density of PSD-95-containing synapses in cultured primary neurons.

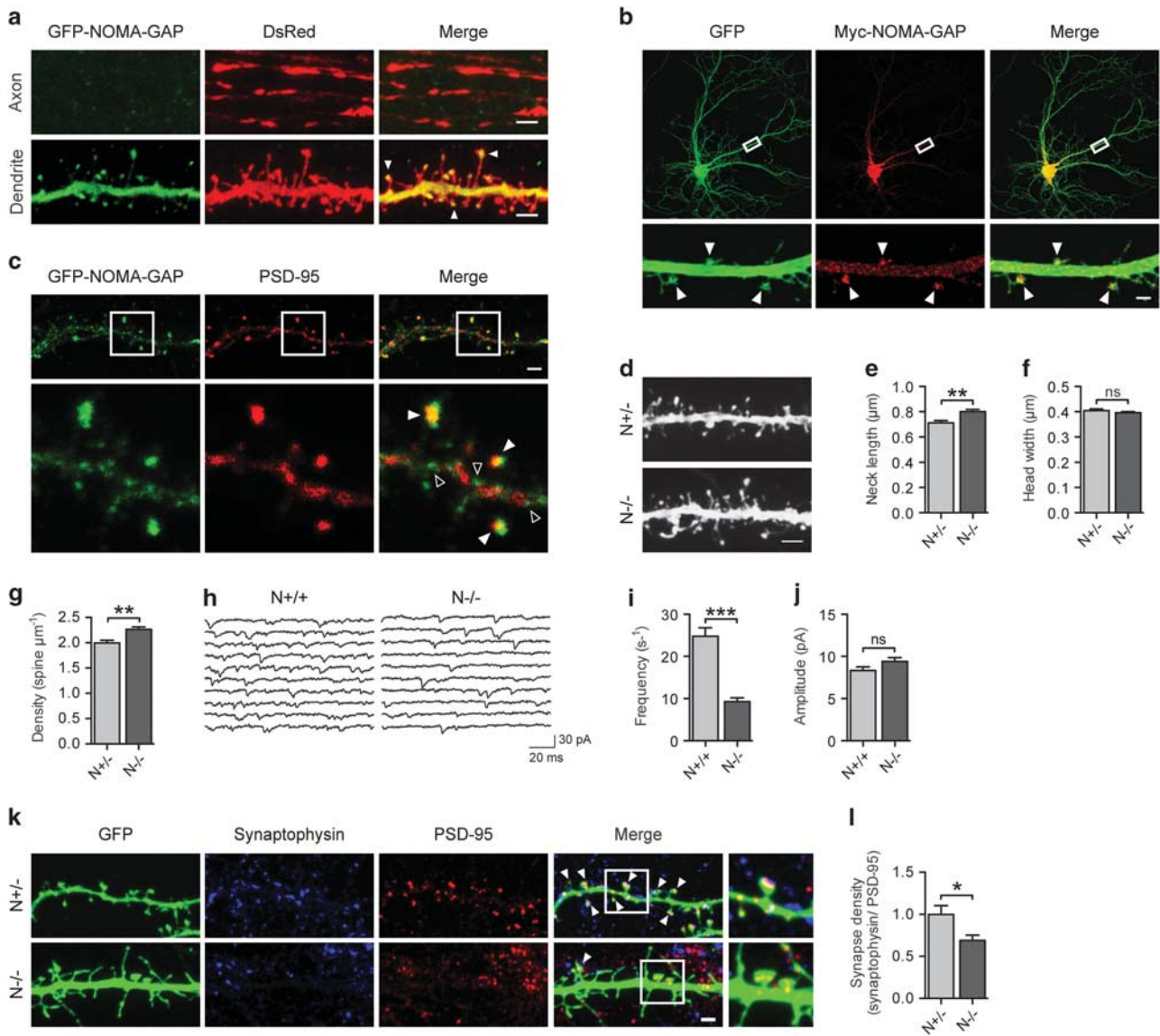


**Figure 2.** NOMA-GAP localizes to dendrites and regulates dendritic spine development. **(a)** NOMA-GAP preferentially targets to dendrites. Green fluorescent protein (GFP)-tagged NOMA-GAP was co-expressed with DsRed in layer 2/3 pyramidal neurons *in vivo* following *in utero* electroporation (IUE) at E15.5. Segments of axons (imaged at the Corpus Callosum) and basal dendrites of electroporated neurons were imaged in cortical slices of 23-day-old (P23) mice. The images were taken under saturating conditions for the dendritic compartment and using the same settings for both axonal and dendritic compartments. Scale bar = 2  $\mu\text{m}$ . **(b)** NOMA-GAP accumulates at dendritic spine heads. Myc-tagged NOMA-GAP was expressed in DIV 14 cortical neurons and analyzed at DIV 20. Scale bar = 2  $\mu\text{m}$ . **(c)** NOMA-GAP colocalizes with PSD-95 at spine heads but not in the dendritic shaft. GFP-tagged NOMA-GAP was expressed in wild-type cortical neurons at DIV 10 and its localization relative to endogenous PSD-95 analyzed at DIV 20. Filled arrows point at colocalized proteins at spine heads and empty arrows at NOMA-GAP puncta along the dendritic shaft. Scale bar = 2  $\mu\text{m}$ . **(d-g)** NOMA-GAP-deficient upper layer cortical neurons show increased spine neck length and spine density in the mouse brain. **(d)** Segments of basal dendrites of layer 2/3 pyramidal neurons expressing eGFP were visualized at P23 following IUE at E15.5. Scale bar = 2  $\mu\text{m}$ . **(e)** Mean length of spine necks.  $n = 615$  N<sup>+/+</sup>,  $765$  N<sup>-/-</sup> spines, Mann-Whitney U-test,  $P = 0.0050$ . **(f)** Mean width of spine head.  $n = 615$  N<sup>+/+</sup>,  $765$  N<sup>-/-</sup>. Mann-Whitney U-test,  $P > 0.05$ . **(g)** Mean spine density.  $n = 13$  N<sup>+/+</sup>,  $14$  N<sup>-/-</sup> dendritic segments of approximate length of 40  $\mu\text{m}$ .  $t$ -test,  $P = 0.0011$ . **(h-j)** Altered electrophysiological properties of NOMA-GAP-deficient neurons in brain slices. **(h)** Continuous voltage clamp recording sequences of 2-s spontaneous postsynaptic activity in principal layer 2/3 somatosensory neurons at a holding of -60 mV broken up to 200 ms periods and arranged vertically. Population data on frequency **(i)** and amplitude **(j)** averaged over at least 3 min in layer 2/3 neurons of NOMA-GAP-deficient and wild-type animals.  $n = 20$  N<sup>+/+</sup> and  $23$  N<sup>-/-</sup> neurons.  $P_{\text{freq}} < 0.000001$ ;  $P_{\text{amp}} = 0.1$ ; decay (37%) N<sup>-/-</sup>:  $5.0 \pm 0.4$  ms ( $n = 23$ ), N<sup>+/+</sup>:  $4.8 \pm 0.3$  ms,  $P = 0.70$ ; membrane potential N<sup>-/-</sup>:  $-71.8 \pm 1.3$  mV, N<sup>+/+</sup>:  $-72.5 \pm 1.3$  mV,  $P = 0.72$ ; input resistance N<sup>-/-</sup>:  $234.6 \text{ M}\Omega \pm 17.0$ , N<sup>+/+</sup>:  $162. \text{ M}\Omega \pm 14.2$ ,  $P = 0.0026$ . **(k-l)** Decrease in the number of PSD-95-containing synapses in NOMA-GAP-deficient neurons. **(k)** Segments of dendrites from cultured cortical neurons expressing eGFP and stained for the presynaptic marker synaptophysin and the postsynaptic marker PSD-95 were visualized at DIV 20. Arrowheads mark opposed synaptophysin and PSD-95 staining. Scale bar = 2  $\mu\text{m}$ . **(l)** Mean synapse density.  $n = 15$  N<sup>+/+</sup>,  $12$  N<sup>-/-</sup> dendritic segments.  $t$ -test,  $P = 0.0244$ .

Loss of NOMA-GAP thus interferes with dendritic spine development and results in an increase in immature dendritic spines and defective synaptic transmission in upper layer cortical neurons.

Regulation of Cdc42 is not involved in NOMA-GAP-mediated control of autism-associated social behavior or dendritic spine maturation. Previously, we demonstrated that NOMA-GAP shows GTPase-activating activity specifically toward the Rho family member Cdc42.<sup>26</sup> Furthermore, we demonstrated that both the elevated Cdc42 activity as well as the defective dendritic branching and neocortical thinning resulting from loss of NOMA-GAP expression in the mouse, could be restored by heterozygous deletion of a floxed Cdc42 gene in postmitotic neurons of the mouse cortex using a Nex1 promoter-driven Cre recombinase.<sup>14</sup>

We used these mouse lines to address whether altered social behavior is dependent on regulation of Cdc42 signaling downstream of NOMA-GAP in the neocortex (Figure 3). The three-chambered task showed that heterozygous deletion of Cdc42 in NOMA-GAP-deficient cortical postmitotic neurons fails to improve social preference (Figure 3a) or recognition (Figure 3b).

We then addressed the role of Cdc42 in NOMA-GAP-mediated regulation of spine morphology. NOMA-GAP regulates the length of dendritic spine necks *in vivo* and *in vitro* (Figures 2d and e and Supplementary Figures S5A and B). *In vivo* heterozygous (Figures 3c and d) or homozygous (Supplementary Figures S5E and H) deletion of Cdc42 in postmitotic neurons, however, fails to restore dendritic spine neck length in NOMA-GAP-deficient mice, suggesting that regulation of Cdc42 by NOMA-GAP is not required for spine maturation. To further investigate this surprising finding, we asked whether we could restore spine morphology *in vivo* in NOMA-GAP-deficient mice by expression of wild-type NOMA-GAP or a mutant of NOMA-GAP that lacks the RhoGAP domain (delRhoGAP; Figures 3g and j, Supplementary Figures S5I and L). Expression of wild-type NOMA-GAP in a subset of cortical neurons of NOMA-GAP-deficient mice, restored dendritic spine neck length (Figure 3h; Supplementary Figure S5J), confirming that the observed spine phenotype is cell autonomous. More importantly, expression of a NOMA-GAP mutant that lacks the RhoGAP domain also restored normal spine morphology in NOMA-GAP-deficient neurons *in vivo* (Figure 3h, Supplementary Figure S5J), suggesting that modulation of Cdc42 signaling is not the primary mechanism by which NOMA-GAP regulates spine maturation. In line with this, whole-cell recordings in cortical slices revealed that reduction of Cdc42 activity in NOMA-GAP-deficient neurons had no effect on the reduced frequency or on the amplitude of sPSCs (Figures 3k and m).

Together, these data lead to the conclusion that NOMA-GAP is essential for normal dendritic spine morphology, synaptic function and for social behavior, and that these processes do not exclusively rely on NOMA-GAP-mediated regulation of Cdc42. Instead, other functions of NOMA-GAP must substantially contribute to these important processes.

#### Interaction and cross-regulation of NOMA-GAP and PSD-MAGUK family members

NOMA-GAP can act as an adaptor protein to recruit multiple signaling molecules.<sup>26</sup> As NOMA-GAP colocalizes with PSD-95 at dendritic spine heads, we assessed whether these proteins interact *in vivo* (Figure 4a). Immunoprecipitates of endogenous NOMA-GAP from cortical lysates of adult wild-type mice showed co-immunoprecipitation of endogenous PSD-95 with NOMA-GAP (Figure 4a). We could also co-immunoprecipitate tagged NOMA-GAP and PSD-95 proteins overexpressed in HEK 293 cells, which lack NOMA-GAP, PSD-95 or other synaptic components (Figures 4b and f). In addition, we observed interaction of NOMA-GAP with other MAGUK family proteins, namely with DLG2/PSD-93 and

DLG3/SAP102 but not with DLG1/SAP97 (Figure 4b). Deletion constructs, revealed that interaction of PSD-95 with NOMA-GAP does not require the PX-like, SH3 or the RhoGAP domains of NOMA-GAP (Figure 4d) but involves sequences that include a serine-proline-rich region that is strongly conserved across species (Supplementary Figure S8). While the article was in preparation, another group also reported interaction of PSD-95 with multiple domains of human NOMA-GAP isoform 1,<sup>27</sup> suggesting that other domains may also contribute to the interaction. The NOMA-GAP interaction site on PSD-95, on the other hand, maps to the C-terminus of PSD-95 that contains the SH3 and guanylate kinase domains (Figures 4e and f). Mutation of residue 460 in the SH3 domain (L460P), a mutation that is thought to open up the configuration of PSD-95,<sup>28,29</sup> enhanced binding. This suggests that the configurational state of PSD-95 and potentially the interaction with other proteins may influence association with NOMA-GAP (see also Rademacher *et al.*<sup>30</sup>). Furthermore, expression of NOMA-GAP induced the translocation of both full-length PSD-95 and the SH3-guanylate kinase region, but not of the PDZ1-3 region, to the plasma membrane when co-expressed in HEK 293 cells (Figures 4g and h).

We then analyzed whether NOMA-GAP is required for PSD-95 localization in cortical neurons (Figures 4 and j). In wild-type neurons, PSD-95 is strongly concentrated at the head of dendritic spines. NOMA-GAP-deficient neurons, however, show an increase in dendritic spines with PSD-95 puncta not only at the spine head but also aberrantly along the neck region (Figure 4j).

The function of MAGUK family proteins is regulated by a number of post-translational modifications including phosphorylation of tyrosine and serine residues.<sup>31–35</sup> Analysis of the phosphorylation state of PSD-95 in NOMA-GAP-deficient and wild-type mouse cortices showed that loss of NOMA-GAP resulted in a striking increase in PSD-95 phosphorylated at serine 295 (pSer295-PSD-95; Figures 5a and b). The levels of tyrosine-phosphorylated PSD-95, however, were not significantly altered (Figures 5c and d). Previous reports have found that pSer295-PSD-95 specifically localizes to synapses.<sup>34</sup> Consistent with this, we observed localization of pSer295-PSD-95 at the heads of dendritic spines in wild-type cortical neurons (Figure 5e). Analysis of the intensity of pSer295-PSD-95 staining in the dendrites of NOMA-GAP-deficient and control neurons confirmed the robust upregulation of pSer295 PSD-95 upon loss of NOMA-GAP (Figure 5f). Remarkably, loss of NOMA-GAP leads to the strong mislocalization of pSer295-PSD-95, away from the spine and into the dendritic shaft (Figures 5e and g). These data indicate that NOMA-GAP regulates PSD-95 phosphorylation and, moreover, that it is necessary for the correct subcellular localization of pSer295-PSD-95. The data also suggest that serine phosphorylation per se is insufficient for correct synaptic localization of PSD-95.

As the binding site of PSD-95 is close to the RhoGAP domain, we also considered the possibility that interaction with PSD-95 could regulate the Cdc42-GAP activity of NOMA-GAP. NOMA-GAP was expressed in HEK 293 cells in the presence or absence of PSD-95 (Figure 5h). Cdc42 activation and thus downstream activation of serine/threonine kinases PAK1/2 was achieved by stimulation with epidermal growth factor. As expected, expression of NOMA-GAP inhibited activation of PAK1/2. Co-expression of increasing amounts of PSD-95, however, counteracted NOMA-GAP-mediated inhibition of PAK1/2 activation. Activation of ERK1/2 MAP kinase by epidermal growth factor was not affected by expression of either NOMA-GAP or PSD-95. Interaction with PSD-95 can thus negatively regulate the Cdc42-GAP activity of NOMA-GAP.

Surface expression of AMPAR is dependent on NOMA-GAP. PSD-95 regulates the synaptic localization of a number of important postsynaptic channels, in particular the AMPA glutamate receptor (AMPA).<sup>36</sup> Aberrant subcellular localization of

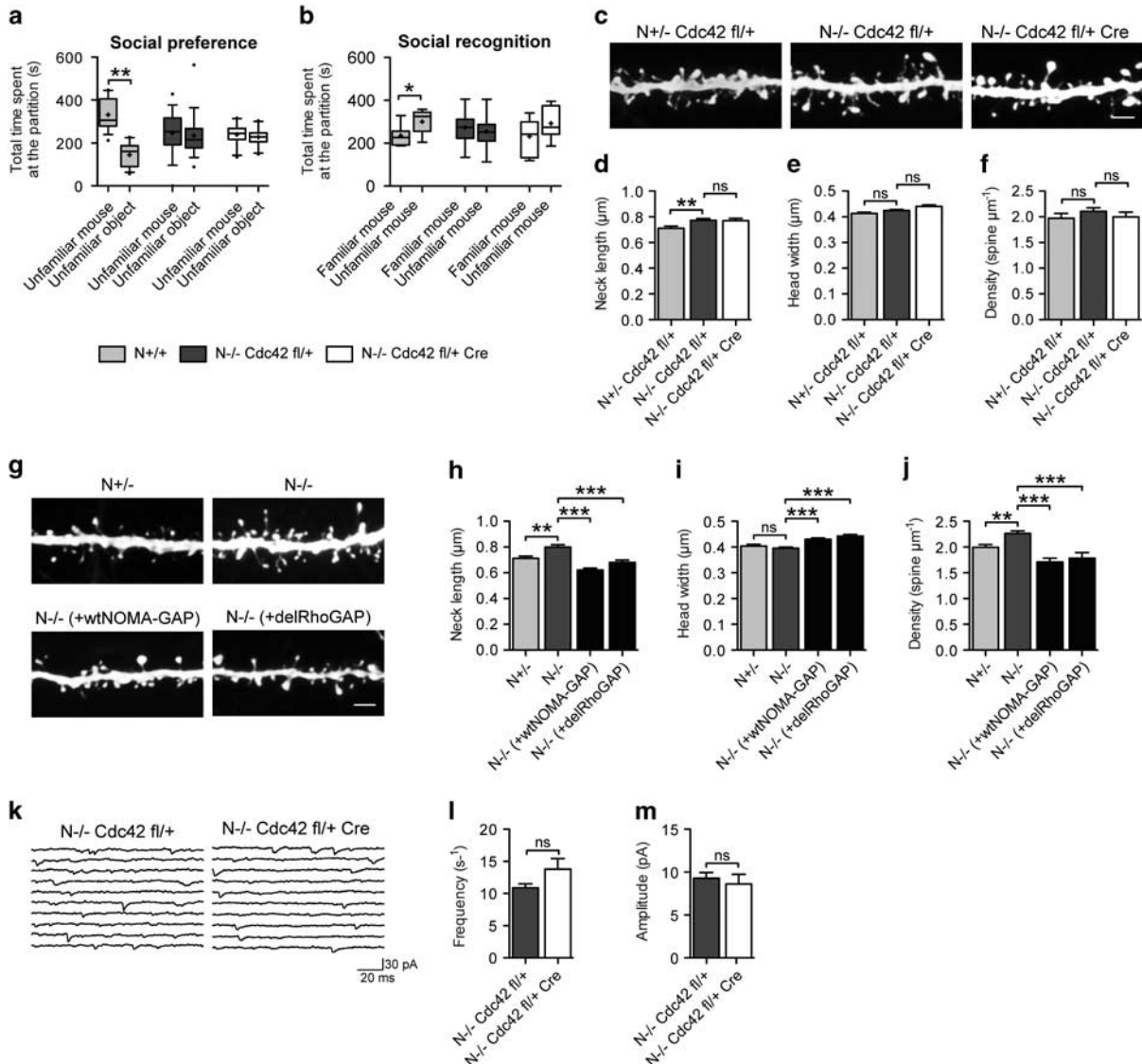


**Figure 3.** Regulation of Cdc42 signaling downstream of NOMA-GAP is not required for NOMA-GAP-regulated aspects of autism-associated social behavior, spine maturation or synaptic transmission. **(a, b)** Restoration of Cdc42 signaling levels does not restore social preference **(a)** or social recognition **(b)** in NOMA-GAP-deficient mice. NOMA-GAP-deficient mice were crossed to Nex1-Cre and floxed Cdc42 mouse lines as described previously.<sup>14</sup> N+/+, N-/- Cdc42 fl/+ and N-/- Cdc42 fl/+ cre/+ male mice were tested in the three-chambered apparatus as described in Figure 1. ( $n = 14$  N+/+ Cdc42 fl/+; 18 N-/- Cdc42 fl/+; 10 N-/- Cdc42 fl/+ cre/+). Non-parametric test, paired values, Wilcoxon test (one-sided tests):  $P_{\text{Social preference}} < 0.005$  (as normal approximation of  $W = 3.3$ );  $P_{\text{Social recognition}} < 0.025$  (as normal approximation of  $W = 2.17$ ). **(c-f)** Heterozygous deletion of Cdc42 fails to restore spine morphology in NOMA-GAP-deficient neurons *in vivo*. **(c)** Segments of basal dendrites of layer 2/3 pyramidal neurons expressing eGFP were visualized at P23 following IUE of littermate N-/- Cdc42 fl/+, N+/+ Cdc42 fl/+ and N-/- Cdc42 fl/+ Nex1-Cre animals at E15.5. Scale bar = 2 µm. **(d)** Mean length of spine neck.  $n = 763$  N+/+ Cdc42 fl/+; 1004 N-/- Cdc42 fl/+; 746 N-/- Cdc42 fl/+ cre spines analyzed. Mann-Whitney *U*-test,  $P_{\text{N+/+ Cdc42 fl/+ vs N-/- Cdc42 fl/+}} = 0.0051$ . **(e)** Mean width of spine head.  $n = 763$  N+/+ Cdc42 fl/+; 1004 N-/- Cdc42 fl/+; 746 N-/- Cdc42 fl/+ cre spines. Mann-Whitney *U*-test. **(f)** Mean spine density.  $n = 14$  N+/+ Cdc42 fl/+; 18 N-/- Cdc42 fl/+; 13 N-/- Cdc42 fl/+ cre dendritic segments of approximate length of 40 µm. *t*-test. **(g-j)** Regulation of *in vivo* spine morphology by NOMA-GAP does not require RhoGAP activity. **(g)** Segments of basal dendrites of layer 2/3 pyramidal neurons expressing eGFP alone (see Figure 2d) or eGFP together with wild-type NOMA-GAP (wtNOMA-GAP) or a RhoGAP-deletion mutant of NOMA-GAP (delRhoGAP) visualized at P23 following IUE at E15.5. Scale bar = 2 µm. **(h)** Mean length of spine neck.  $n = 824$  N-/- (+wtNOMA-GAP); 782 N-/- (+delRhoGAP) spines analyzed. Mann-Whitney *U*-test,  $P_{\text{N-/- vs N-/- (+wtNOMA-GAP)}} < 0.0001$ ;  $P_{\text{N-/- vs N-/- (+delRhoGAP)}} < 0.0001$ ;  $P_{\text{N+/+ vs N-/- (+wtNOMA-GAP)}} < 0.0001$ ;  $P_{\text{N+/+ vs N-/- (+delRhoGAP)}} = 0.048$ ;  $P_{\text{N-/- (+wtNOMA-GAP) vs N-/- (+delRhoGAP)}} = 0.038$ . **(i)** Mean width of spine head.  $n = 824$  N-/- (+wtNOMA-GAP); 782 N-/- (+delRhoGAP). Mann-Whitney *U*-test  $P_{\text{N-/- vs N-/- (+wtNOMA-GAP)}} < 0.0001$ ;  $P_{\text{N-/- vs N-/- (+delRhoGAP)}} < 0.0001$ ;  $P_{\text{N+/+ vs N-/- (+wtNOMA-GAP)}} < 0.0001$ ;  $P_{\text{N+/+ vs N-/- (+delRhoGAP)}} < 0.0001$ ;  $P_{\text{N-/- (+wtNOMA-GAP) vs N-/- (+delRhoGAP)}} = 0.16$ . **(j)** Mean spine density.  $n = 13$  N-/- (+wtNOMA-GAP); 13 N-/- (+delRhoGAP) dendritic segments of approximate length of 40 µm. *t*-test,  $P_{\text{N-/- vs N-/- (+wtNOMA-GAP)}} < 0.0001$ ;  $P_{\text{N-/- vs N-/- (+delRhoGAP)}} = 0.0005$ ;  $P_{\text{N+/+ vs N-/- (+wtNOMA-GAP)}} = 0.0044$ ;  $P_{\text{N+/+ vs N-/- (+delRhoGAP)}} = 0.098$ ;  $P_{\text{N-/- (+wtNOMA-GAP) vs N-/- (+delRhoGAP)}} = 0.59$ . **(k-m)** Heterozygous deletion of Cdc42 does not alter the electrophysiological properties of NOMA-GAP-deficient neurons. **(k)** Spontaneous postsynaptic activity in principal layer 2/3 somatosensory NOMA-GAP-deficient neurons with different amounts of Cdc42 was recorded in brain slices as described in Figure 2. Reducing Cdc42 neither rescued the frequency **(l)** nor changed the amplitude **(m)** of spontaneously occurring postsynaptic currents averaged over recording periods of at least 3 min. Input resistance N-/- Cdc42 fl/+, 192.0 MΩ ± 21.0, N-/- Cdc42 fl/+ cre: 182.9 MΩ ± 21.9.  $n = 12$  N-/- Cdc42 fl/+, 11 N-/- Cdc42 fl/+ Nex1 cre neurons. Mann-Whitney *U*-test,  $P = 0.76$ .

PSD-95 resulting from loss of NOMA-GAP expression may thus affect the subcellular localization of AMPAR. Staining for total cellular GluR1, one of the AMPAR subunits, in littermate control and NOMA-GAP-deficient mature cortical neurons showed no alteration in the levels of this protein upon loss of NOMA-GAP (Figures 5i and j). However, when we selectively stained for GluR1 found at the plasma membrane of the cells, we observed a pronounced loss (over 50%) of surface GluR1 in the dendrites of NOMA-GAP-deficient neurons (Figures 5k and l). These results were confirmed by biotinylation of surface proteins in NOMA-GAP-deficient and littermate control primary neurons, where we again

observed a drastic loss of GluR1 at the plasma membrane of NOMA-GAP-deficient neurons (Figures 5m and n). NOMA-GAP is therefore essential for the expression of AMPAR at the plasma membrane.

**DISCUSSION**

Abnormalities in dendritic tree and spine morphology are commonly associated with neuropsychiatric developmental disorders such as ASD and schizophrenia.<sup>1,37</sup> Understanding the molecular reasons for these abnormalities and linking these to the

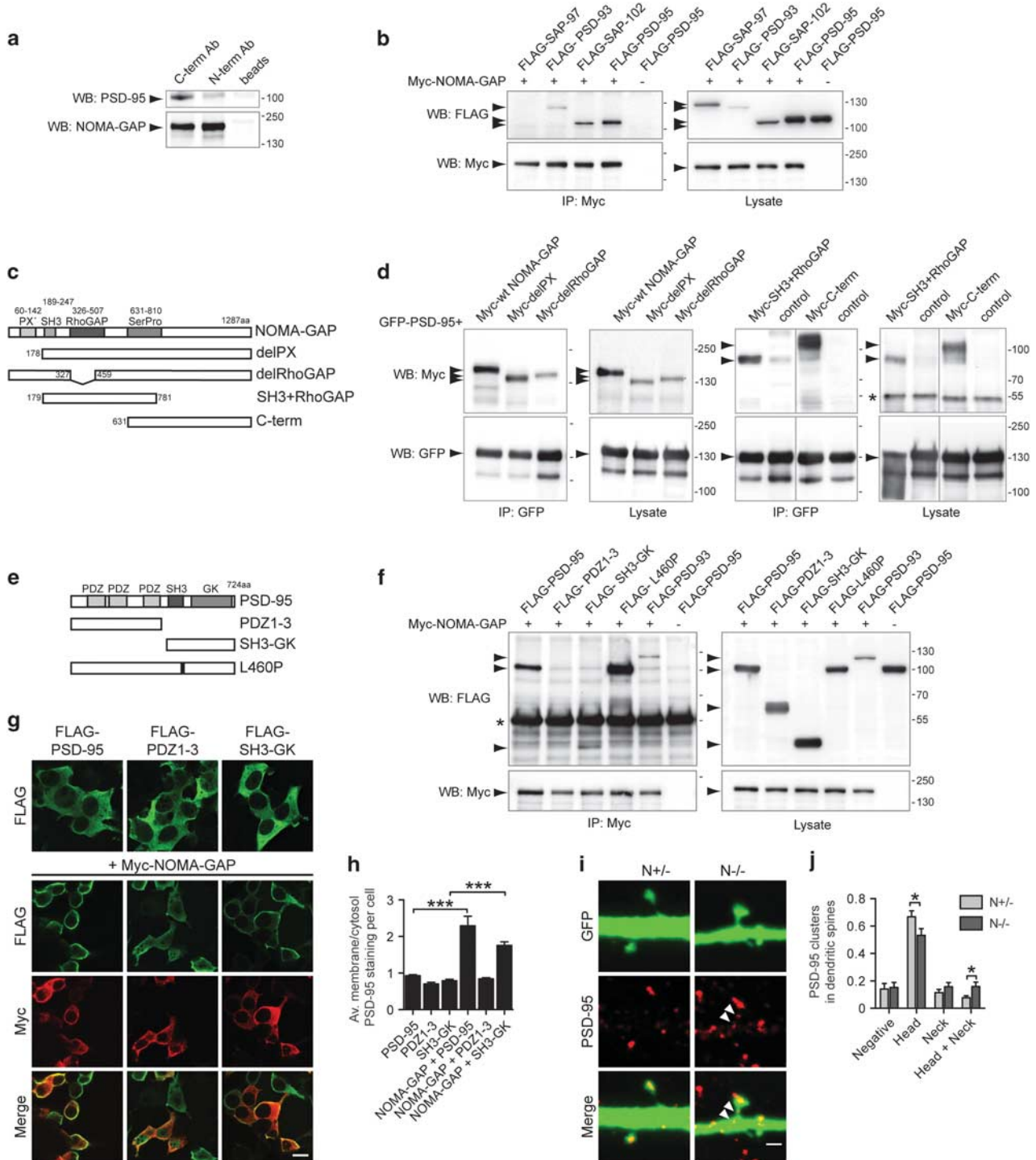


Figure 4. For caption see page 1128.

disease phenotype has not, however, been straightforward. We show that loss of NOMA-GAP, a GAP for the Rho family member Cdc42 and a multiadaptor signaling molecule expressed in postmitotic neurons, leads to autism-like alterations in social behavior. NOMA-GAP-deficient male mice show normal general behavior, health, motoric and sensory function but demonstrate both lack of interest in an unfamiliar mouse and a very pronounced inability to differentiate a familiar and a novel mouse. These key markers for autism-like behavior in the mouse<sup>17</sup> reflect the characteristic poor performance of individuals with neuropsychiatric developmental disorders, such as ASD and schizophrenia, in social communication and interaction tests including facial recognition tests.<sup>38,39</sup> Interestingly, and in parallel with these human conditions, NOMA-GAP-deficient mice show normal explorative behavior, indicating a very restricted defect in social interaction. Furthermore, social interaction deficits are restricted to male NOMA-GAP-deficient mice. Female NOMA-GAP-deficient mice, on the other hand, show signs of increased anxiety in a variety of tests. Multiple patient comparison studies have identified gender-associated differences in the outward expression of neuropsychiatric developmental disorders such as ASD and schizophrenia. These have been attributed to the influence of sex hormones on behavior and development (reviewed in Seeman and Lang<sup>40</sup> and Baron-Cohen *et al.*<sup>41</sup>). Although neuropsychiatric developmental disorders show a strong gender bias, sexual dimorphism has been reported in only a few mouse models. These include mice deficient in the schizophrenia risk-associated gene *ZDHHC8* that show female-specific deficit in prepulse inhibition<sup>42</sup> and mice deficient in the ASD-associated Shank3 protein that show a male-specific increase in repetitive self-grooming.<sup>43</sup> Elevated anxiety is one of the most common comorbidities with neuropsychiatric developmental disorders, its prevalence being higher in affected females.<sup>44</sup> Indeed, differences in outward expression of these diseases have been suggested to result in the misdiagnosis of ASD-affected women and girls, most often with conditions such as borderline personality disorder, anxiety disorder or depression.<sup>45</sup> NOMA-GAP-deficient mice thereby mirror human neuropsychiatric developmental disorders in the gender-differentiated expression of the behavioral phenotype, making this a mouse model of particular relevance for future studies in this direction.

ASD and schizophrenia have been suggested to result from defective synapse maturation and indeed defective spine morphology has been described in human patients.<sup>1,46</sup> Maturation of synapses during postnatal development requires the

recruitment of functional AMPARs to the postsynaptic site, a process in which PSD-95 has a critical role.<sup>47–49</sup> Loss of PSD-95 leads to a higher number of synapses that lack AMPARs (silent-synapses<sup>25,48,50,51</sup>) and is associated with increase dendritic spine length.<sup>48,52</sup> Like other candidate molecules for neuropsychiatric disorders,<sup>20</sup> NOMA-GAP is a postsynaptic protein that is required for spine maturation and synaptic transmission. Furthermore, NOMA-GAP also directly interacts with multiple MAGUK proteins and is, moreover, an important regulator of PSD-95 function in the mouse brain. Both subcellular location and phosphorylation of PSD-95, factors that are critical for normal dendritic spine maturation, are dependent on NOMA-GAP. Serine 295 phosphorylation of PSD-95 was previously shown to increase the levels of PSD-95 at synapses and thereby to promote recruitment of AMPAR and enhancement of postsynaptic currents.<sup>34</sup> Phosphorylation of PSD-95 at serine 295 is markedly increased in the cortex and in dissociated neurons of NOMA-GAP-deficient mice. pSer295 PSD-95, however, is strikingly mislocalized in NOMA-GAP-deficient neurons away from the spine head and toward the dendritic shaft. Together this suggests that NOMA-GAP is an important regulator of both serine 295 phosphorylation and the subcellular localization of PSD-95.

Like PSD-95-deficient neurons, NOMA-GAP-deficient neurons also show defective synaptic transmission with strongly reduced mEPSC frequency but no alteration in amplitude. This phenotype has been attributed to the decrease in the number of AMPAR-containing synapses and thus of AMPAR transmission in PSD-95-deficient neurons.<sup>48</sup> Indeed, we show that surface expression of the glutamate AMPAR is strongly compromised in NOMA-GAP-deficient neurons, providing a likely molecular basis for defective synaptic transmission and altered behavior of these mice. Of note, in what may be a recurring mechanism in the development of ASD, the ASD-associated Neurexin/Neuroigin adhesion pair was recently shown to regulate AMPAR trafficking and presence at synapses through PSD-95.<sup>53,54</sup>

Interestingly, our data show that regulation of Cdc42 by NOMA-GAP in the neocortex is not absolutely required for spine maturation, synaptic transmission or NOMA-GAP-dependent aspects of autism-associated social behavior. In terms of the formation of new spines, loss of NOMA-GAP leads to an increase in spine density *in vivo* but not in cultured neurons, suggesting that extracellular conditions may influence this process. Contradictory results have also been reported by others, with respect to the role of Cdc42 and/or NOMA-GAP in regulating the formation of new spines.<sup>27,55–57</sup> Clearly, further studies, including both *in vivo* and

**Figure 4.** NOMA-GAP interacts with MAGUK family proteins and regulates the subcellular localization of PSD-95. **(a)** NOMA-GAP exists in an *in vivo* complex with PSD-95. Endogenous NOMA-GAP was immunoprecipitated from lysates of adult mouse cortices using a C or N-terminal directed antibody. Immunoprecipitates were analyzed for the presence of endogenous PSD-95. **(b)** NOMA-GAP can interact with multiple MAGUK family proteins. FLAG-tagged forms of the MAGUK family proteins DLG1/SAP97, DLG2/PSD-93, DLG3/SAP102 and DLG4/PSD-95 were co-expressed with Myc-tagged NOMA-GAP in HEK 293 cells. The presence of FLAG-tagged MAGUK proteins in anti-Myc immunoprecipitates was detected by western blotting as indicated. **(c)** Schematic representation of the NOMA-GAP deletion constructs used. **(d)** Interaction of PSD-95 with NOMA-GAP maps to a serine–proline-rich region in NOMA-GAP. Green fluorescent protein (GFP)-tagged PSD-95 and Myc-tagged forms of NOMA-GAP deletion constructs described in **(c)** were expressed in HEK 293 cells. Proteins were immunoprecipitated as indicated. **(e)** Schematic representation of the PSD-95 deletion constructs used. **(f)** Interaction of NOMA-GAP with PSD-95 maps to the C-terminal SH3-guanylate kinase (GK) region of PSD-95. Myc-tagged NOMA-GAP was co-expressed with FLAG-tagged PSD-95 deletion constructs in HEK 293 cells. Anti-Myc immunoprecipitates were probed for co-immunoprecipitating FLAG-tagged PSD-95. Antibody heavy chain band is marked with an asterisk. Scale bar = 2  $\mu$ m. **(g–h)** NOMA-GAP induces translocation of full-length or the SH3-GK region of PSD-95 to the plasma membrane. FLAG-tagged PSD-95 constructs (shown in green) were expressed alone or together with Myc-tagged NOMA-GAP (shown in red) in HEK 293 cells **(g)**. Localization of these proteins was detected by immunofluorescent staining against the respective tags. Scale bar = 20  $\mu$ m. **(h)** Average ratio of PSD-95 staining intensity at the membrane to PSD-95 in the cytoplasm per cell. The Kruskal–Wallis one-way analysis of variance by ranks test was used to compare the different samples.  $n_{\text{PSD-95}} = 32$ ,  $n_{\text{PDZ}} = 11$ ,  $n_{\text{SH3-GK}} = 12$ ,  $n_{\text{NOMA-GAP+PSD-95}} = 19$ ,  $n_{\text{NOMA-GAP+PDZ}} = 18$ ,  $n_{\text{NOMA-GAP+SH3-GK}} = 34$ . Mann–Whitney *U*-test  $P_{\text{PSD-95 vs NOMA-GAP+PSD-95}} < 0.0001$ ;  $P_{\text{SH3-GK vs NOMA-GAP+SH3-GK}} < 0.0001$ . **(i–j)** NOMA-GAP regulates the subcellular localization of PSD-95 in cortical neurons. The localization of endogenous PSD-95 (shown in red) within dendritic spines was analyzed by immunofluorescent staining in GFP-expressing NOMA-GAP-deficient and control cortical neurons **(i)**. **(j)** Quantification of the number of spines showing PSD-95 clusters in the dendritic spine head and/or neck.  $n = 13$  N+/-, 12 N-/- dendritic segments of a mean length of 60  $\mu$ m. *t*-tests,  $P_{\text{Head}} = 0.0475$ ;  $P_{\text{Head and Neck}} = 0.0286$ . Scale bar = 1  $\mu$ m.

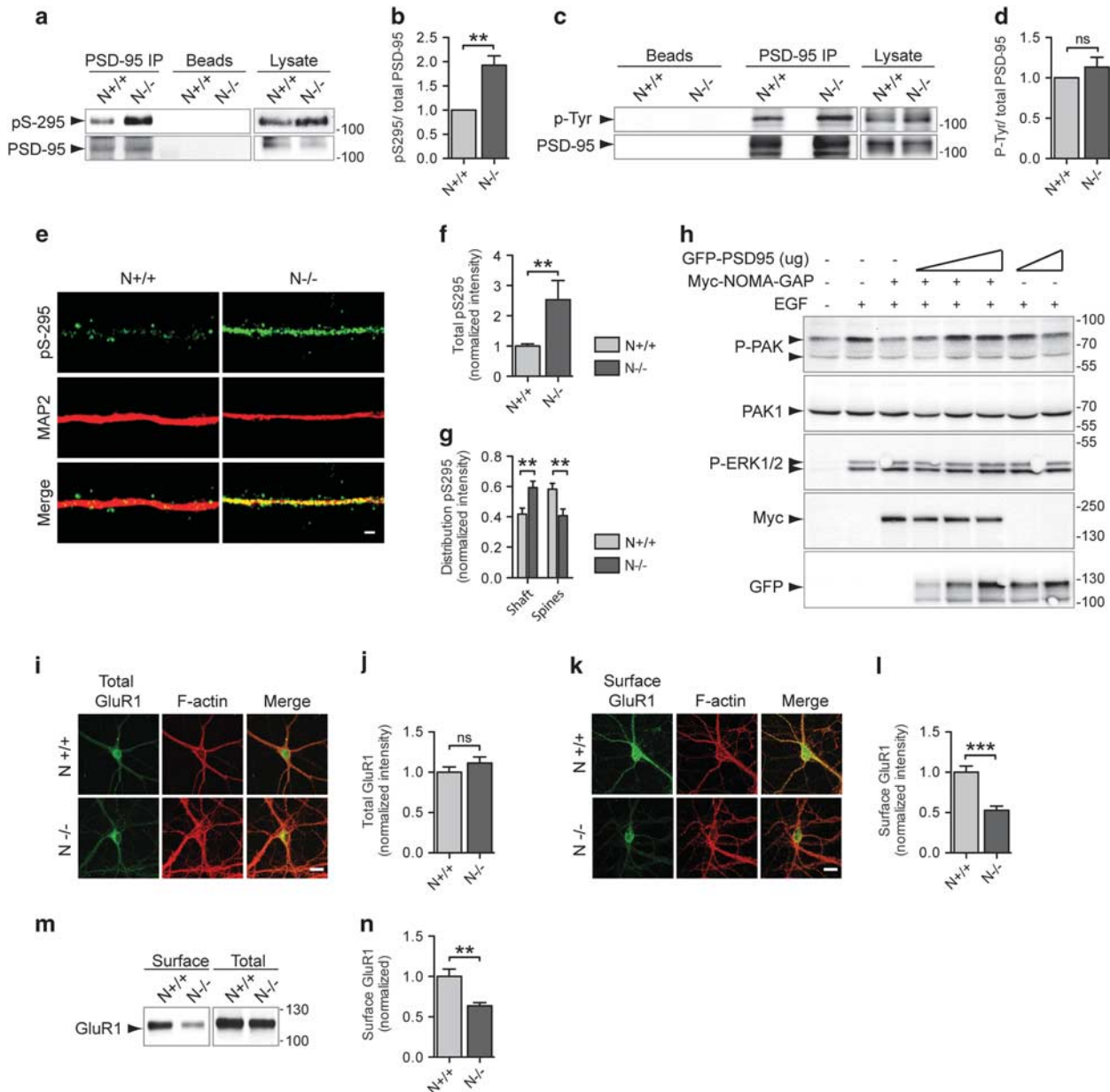


**Figure 5.** PSD-95 function and surface expression of AMPAR are dependent on NOMA-GAP. **(a, b)** NOMA-GAP regulates phosphorylation of PSD-95 at serine 295 *in vivo*. The levels of serine 295 phosphorylation of PSD-95 were analyzed in immunoprecipitates of endogenous PSD-95 and in whole-cell lysates of adult NOMA-GAP-deficient and wild-type mouse cortices **(a)**. **(b)** Quantification of the level of serine 295 phosphorylated PSD-95 (pSer295 PSD-95/total PSD-95) in adult mouse cortex.  $n = 5$ ;  $t$ -test,  $P = 0.009$ . **(c, d)** Tyrosine phosphorylation of PSD-95 is not altered in the cortex of NOMA-GAP-deficient mice. PSD-95 immunoprecipitates from whole-cell lysates of adult NOMA-GAP-deficient and wild-type mouse cortices were analyzed for tyrosine phosphorylation as indicated. Quantification of specific tyrosine phosphorylation levels is shown in **(d)**.  $n = 4$ ;  $t$ -test. **(e-g)** Serine 295 phosphorylated PSD-95 is mislocalized in NOMA-GAP-deficient neurons. **(e)** NOMA-GAP-deficient and wild-type mature cortical neurons (DIV 22) derived from littermate animals were stained for Ser 295 phosphorylated PSD-95 (shown in green) and for the dendritic marker MAP2 (shown in red). Scale bar = 2  $\mu$ m. **(f)** Quantification of the average intensity of Ser 295 phosphorylated PSD-95 in the dendrites of NOMA-GAP-deficient and control neurons.  $n = 10$  N+/+, 10 N-/- . Mann-Whitney  $U$ -test,  $P = 0.0052$ . **(g)** Localization of pS295 PSD-95 in the dendrites of NOMA-GAP-deficient and control neurons.  $n = 10$  N+/+, 10 N-/- .  $t$ -test  $P_{Shaft} = 0.0078$ ,  $P_{Spines} = 0.0078$ . **(h)** PSD-95 inhibits the Cdc42-GAP activity of NOMA-GAP. Myc-tagged NOMA-GAP was expressed in HEK 293 cells in the absence or presence of increasing levels of GFP-tagged PSD-95. Endogenous PAK phosphorylation was induced by a 10 min stimulation with 100 ng/ml epidermal growth factor. **(i-j)** Total levels of GluR1 are not affected by loss of NOMA-GAP. Permeabilized NOMA-GAP-deficient and littermate wild-type cortical neurons were stained in parallel for endogenous GluR1 (shown in green) and F-actin (shown in red) at DIV 22 **(i)**. Scale bar = 20  $\mu$ m. **(j)** Quantification of total GluR1 staining.  $n = 12$  N+/+, 12 N-/- ,  $t$ -test. **(k-l)** Loss of surface GluR1 in NOMA-GAP-deficient neurons. **(k)** NOMA-GAP-deficient and littermate wild-type primary cortical neurons were stained at DIV 22 for surface expression of endogenous GluR1 (shown in green) and F-actin (shown in red). Scale bar = 20  $\mu$ m. **(l)** Quantification of the intensity of surface GluR1 expression on dendrites of NOMA-GAP-deficient and wild-type cortical neurons.  $n = 10$  N+/+ and 10 N-/- cells.  $t$ -test,  $P < 0.0001$ . **(m, n)** NOMA-GAP regulates the levels of surface-expressed GluR1 in cortical neurons. **(m)** Proteins expressed on the outer membrane of cultured mature primary cortical neurons (DIV 22) derived from NOMA-GAP-deficient or littermate wild-type embryos were labeled by biotinylation. Biotinylated proteins were precipitated and the levels of labeled and total GluR1 analyzed by western blotting. **(n)** Quantification of surface biotinylated GluR1 in NOMA-GAP-deficient and control neurons.  $n = 9$  N+/+, 10 N-/- ,  $t$ -test,  $P = 0.0015$ .

*in vitro* analyses, will be necessary to elucidate the mechanisms by which new spines are initiated. Indeed, recent data using *in vivo* conditional deletion of the *Cdc42* gene suggests that the role, if any, for *Cdc42* in this process is dependent on the brain region.<sup>58</sup>

The interaction with PSD-95 negatively regulates the GAP activity of NOMA-GAP. This raises the possibility that there may be two pools of NOMA-GAP with different signaling functions in neurons: one located at the dendritic spine head where these two proteins colocalize and the other in the dendritic shaft where they do not. In this latter compartment, NOMA-GAP would be expected to possess higher *Cdc42*-GAP activity, a function, which we previously showed is required for induction of new dendritic branch points.<sup>14</sup> Dendritic spine maturation, however, does not require inhibition of *Cdc42* by NOMA-GAP, and this signaling function may furthermore be actively suppressed by interaction with PSD-95. In fact, *Cdc42* becomes activated in dendritic spines following stimulation and is necessary for synaptic transmission.<sup>59</sup> Activation of *Cdc42* during synaptic transmission, however, differs from that of other RhoGTPases. It is sharply restricted to the dendritic spine head and, unlike other RhoGTPases, does not spread to the spine neck region or to the dendritic shaft, despite similar protein mobility.<sup>59</sup> This raises the possibility that, in the spine head, inhibition of NOMA-GAP by PSD-95 may enable activation of *Cdc42* in this subcellular compartment, whereas unbound NOMA-GAP elsewhere modulates *Cdc42* activation levels and/or prevents expansion of *Cdc42* activity into the dendritic spine neck and shaft.

In summary, in this work we uncover a novel molecular mechanism involving the cross-regulation of the postsynaptic proteins NOMA-GAP and PSD-95 that is required for dendritic spine and synapse development in the mammalian neocortex. Defects in this system are associated with loss of surface AMPAR, defective synaptic transmission and most importantly with autism-like alterations in social behavior in the mouse. Further work is required to assess NOMA-GAP function in patients with neuropsychiatric developmental disorders. This molecular mechanism, however, sheds new light on both how dendritic spine development is regulated but also on the molecular events that lead to autism-like behavior in the animal.

## CONFLICT OF INTEREST

The authors declare no conflict of interest.

## ACKNOWLEDGMENTS

We thank E Tarland for valuable technical support with the animal behavior experiments and for Supplementary Figure S4A and J Schüler for advice on microscopy and E Bessa for help during the revision process. This study was supported by the DFG: RO3497/3-1 (M Rosário); EXC257 NeuroCure (M Rivalan, YW, NR, SAS and VT); SFB665 and Heisenberg program (VT). In addition, SS was funded by the Charité PhD Scholarship and equipment used by US was partially funded by the Sonnenfeld Stiftung.

## REFERENCES

- 1 Penzes P, Cahill ME, Jones KA, VanLeeuwen JE, Woolfrey KM. Dendritic spine pathology in neuropsychiatric disorders. *Nat Neurosci* 2011; **14**: 285–293.
- 2 Zheng CY, Seabold GK, Horak M, Petralia RS. MAGUKs, synaptic development, and synaptic plasticity. *Neuroscientist* 2011; **17**: 493–512.
- 3 Tarpey P, Parnau J, Blow M, Woffendin H, Bignell G, Cox C *et al*. Mutations in the *DLG3* gene cause nonsyndromic X-linked mental retardation. *Am J Hum Genet* 2004; **75**: 318–324.
- 4 Zanni G, van Esch H, Bensalem A, Saillour Y, Poirier K, Castelneau L *et al*. A novel mutation in the *DLG3* gene encoding the synapse-associated protein 102 (SAP102) causes non-syndromic mental retardation. *Neurogenetics* 2009; **11**: 251–255.
- 5 Romorini S, Piccoli G, Jiang M, Grossano P, Tonna N, Passafaro M *et al*. A functional role of postsynaptic density-95-guanylate kinase-associated protein complex in regulating Shank assembly and stability to synapses. *J Neurosci* 2004; **24**: 9391–9404.

- 6 Naisbitt S, Kim E, Tu JC, Xiao B, Sala C, Valtchanoff J *et al*. Shank, a novel family of postsynaptic density proteins that binds to the NMDA receptor/PSD-95/GKAP complex and cortactin. *Neuron* 1999; **23**: 569–582.
- 7 Irie M, Hata Y, Takeuchi M, Ichtchenko K, Toyoda A, Hirao K *et al*. Binding of neurologins to PSD-95. *Science* 1997; **277**: 1511–1515.
- 8 Zhu YC, Li D, Wang L, Lu B, Zheng J, Zhao SL *et al*. Palmitoylation-dependent CDKL5-PSD-95 interaction regulates synaptic targeting of CDKL5 and dendritic spine development. *Proc Natl Acad Sci USA* 2013; **110**: 9118–9123.
- 9 Kunde SA, Rademacher N, Tzschach A, Wiedersberg E, Ullmann R, Kalscheuer VM *et al*. Characterisation of de novo MAPK10/JNK3 truncation mutations associated with cognitive disorders in two unrelated patients. *Hum Genet* 2013; **132**: 461–471.
- 10 Feyder M, Karlsson RM, Mathur P, Lyman M, Bock R, Momenan R *et al*. Association of mouse *Dlg4* (PSD-95) gene deletion and human *DLG4* gene variation with phenotypes relevant to autism spectrum disorders and Williams' syndrome. *Am J Psychiatry* 2010; **167**: 1508–1517.
- 11 Govak EE, Newey SE, Van Aelst L. The role of the Rho GTPases in neuronal development. *Genes Dev* 2005; **19**: 1–49.
- 12 Bennett MR. Schizophrenia: susceptibility genes, dendritic-spine pathology and gray matter loss. *Prog Neurobiol* 2011; **95**: 275–300.
- 13 Toliai KF, Duman JG, Um K. Control of synapse development and plasticity by Rho GTPase regulatory proteins. *Prog Neurobiol* 2011; **94**: 133–148.
- 14 Rosario M, Schuster S, Juttner R, Parthasarathy S, Tarabykin V, Birchmeier W. Neocortical dendritic complexity is controlled during development by NOMA-GAP-dependent inhibition of *Cdc42* and activation of cofilin. *Genes Dev* 2012; **26**: 1743–1757.
- 15 Goebels S, Bormuth I, Bode U, Hermanson O, Schwab MH, Nave KA. Genetic targeting of principal neurons in neocortex and hippocampus of NEX-Cre mice. *Genesis* 2006; **44**: 611–621.
- 16 Schmeisser MJ, Ey E, Wegener S, Bockmann J, Stempel AV, Kuebler A *et al*. Autistic-like behaviours and hyperactivity in mice lacking ProSAP1/Shank2. *Nature* 2012; **486**: 256–260.
- 17 Crawley JN. Mouse behavioral assays relevant to the symptoms of autism. *Brain Pathol* 2007; **17**: 448–459.
- 18 Silverman JL, Yang M, Lord C, Crawley JN. Behavioural phenotyping assays for mouse models of autism. *Nat Rev Neurosci* 2010; **11**: 490–502.
- 19 Moy SS, Nadler JJ, Perez A, Barbaro RP, Johns JM, Magnuson TR *et al*. Sociability and preference for social novelty in five inbred strains: an approach to assess autistic-like behavior in mice. *Genes Brain Behav* 2004; **3**: 287–302.
- 20 Ebert DH, Greenberg ME. Activity-dependent neuronal signalling and autism spectrum disorder. *Nature* 2013; **493**: 327–337.
- 21 Liu H, Nakazawa T, Tezuka T, Yamamoto T. Physical and functional interaction of Fyn tyrosine kinase with a brain-enriched Rho GTPase-activating protein TCGAP. *J Biol Chem* 2006; **281**: 23611–23619.
- 22 Araya R, Vogels TP, Yuste R. Activity-dependent dendritic spine neck changes are correlated with synaptic strength. *Proc Natl Acad Sci USA* 2014; **111**: E2895–E2904.
- 23 Araya R, Jiang J, Eisenthal KB, Yuste R. The spine neck filters membrane potentials. *Proc Natl Acad Sci USA* 2006; **103**: 17961–17966.
- 24 Simkus CR, Stricker C. Properties of mEPSCs recorded in layer II neurones of rat barrel cortex. *J Physiol* 2002; **545**: 509–520.
- 25 Stein V, House DR, Bredt DS, Nicoll RA. Postsynaptic density-95 mimics and occludes hippocampal long-term potentiation and enhances long-term depression. *J Neurosci* 2003; **23**: 5503–5506.
- 26 Rosario M, Franke R, Bednarski C, Birchmeier W. The neurite outgrowth multi-adaptor RhoGAP, NOMA-GAP, regulates neurite extension through SHP2 and *Cdc42*. *J Cell Biol* 2007; **178**: 503–516.
- 27 Kim Y, Ha CM, Chang S. SNX26, a GTPase-activating protein for *Cdc42*, interacts with PSD-95 protein and is involved in activity-dependent dendritic spine formation in mature neurons. *J Biol Chem* 2013; **288**: 29453–29466.
- 28 McGee AW, Bredt DS. Identification of an intramolecular interaction between the SH3 and guanylate kinase domains of PSD-95. *J Biol Chem* 1999; **274**: 17431–17436.
- 29 Shin H, Hsueh YP, Yang FC, Kim E, Sheng M. An intramolecular interaction between Src homology 3 domain and guanylate kinase-like domain required for channel clustering by postsynaptic density-95/SAP90. *J Neurosci* 2000; **20**: 3580–3587.
- 30 Rademacher N, Kunde SA, Kalscheuer VM, Shoichet SA. Synaptic MAGUK multimer formation is mediated by PDZ domains and promoted by ligand binding. *Chem Biol* 2013; **20**: 1044–1054.
- 31 Nada S, Shima T, Yanai H, Husi H, Grant SG, Okada M *et al*. Identification of PSD-93 as a substrate for the Src family tyrosine kinase Fyn. *J Biol Chem* 2003; **278**: 47610–47621.
- 32 Jaffe H, Vinade L, Dosemeci A. Identification of novel phosphorylation sites on postsynaptic density proteins. *Biochem Biophys Res Commun* 2004; **321**: 210–218.

- 33 Zhang J, Petit CM, King DS, Lee AL. Phosphorylation of a PDZ domain extension modulates binding affinity and interdomain interactions in postsynaptic density-95 (PSD-95) protein, a membrane-associated guanylate kinase (MAGUK). *J Biol Chem* 2011; **286**: 41776–41785.
- 34 Kim MJ, Futai K, Jo J, Hayashi Y, Cho K, Sheng M. Synaptic accumulation of PSD-95 and synaptic function regulated by phosphorylation of serine-295 of PSD-95. *Neuron* 2007; **56**: 488–502.
- 35 Perez de Arce K, Varela-Nallar L, Farias O, Cifuentes A, Bull P, Couch BA *et al*. Synaptic clustering of PSD-95 is regulated by c-Abl through tyrosine phosphorylation. *J Neurosci* 2010; **30**: 3728–3738.
- 36 Yudowski GA, Olsen O, Adesnik H, Marek KW, Brecht DS. Acute inactivation of PSD-95 destabilizes AMPA receptors at hippocampal synapses. *PLoS One* 2013; **8**: e53965.
- 37 Kulkarni VA, Firestein BL. The dendritic tree and brain disorders. *Mol Cell Neurosci* 2012; **50**: 10–20.
- 38 Sachs G, Steger-Wuchse D, Kryspin-Exner I, Gur RC, Katschnig H. Facial recognition deficits and cognition in schizophrenia. *Schizophr Res* 2004; **68**: 27–35.
- 39 Sigman M, Spence SJ, Wang AT. Autism from developmental and neuropsychological perspectives. *Annu Rev Clin Psychol* 2006; **2**: 327–355.
- 40 Seeman MV, Lang M. The role of estrogens in schizophrenia gender differences. *Schizophr Bull* 1990; **16**: 185–194.
- 41 Baron-Cohen S, Lombardo MV, Auyeung B, Ashwin E, Chakrabarti B, Knickmeyer R. Why are autism spectrum conditions more prevalent in males? *PLoS Biol* 2011; **9**: e1001081.
- 42 Mukai J, Liu H, Burt RA, Swor DE, Lai WS, Karayiorgou M *et al*. Evidence that the gene encoding ZDHHC8 contributes to the risk of schizophrenia. *Nat Genet* 2004; **36**: 725–731.
- 43 Yang M, Bozdagi O, Scattoni ML, Wohr M, Roulet F, Katz AM *et al*. Reduced excitatory neurotransmission and mild autism-relevant phenotypes in adolescent Shank3 null mutant mice. *J Neurosci* 2012; **32**: 6525–6541.
- 44 Gotham K, Bishop SL, Hus V, Huerta M, Lund S, Buja A *et al*. Exploring the relationship between anxiety and insistence on sameness in autism spectrum disorders. *Autism Res* 2012; **6**: 33–41.
- 45 American Psychiatric Association, Kernberg. Diagnostic and Statistical Manual of Mental Disorders, Fifth Edition, 2013. American Psychiatric Publishing Inc, Arlington, VA, USA.
- 46 Hanse E, Seth H, Riebe I. AMPA-silent synapses in brain development and pathology. *Nat Rev Neurosci* 2010; **14**: 839–850.
- 47 Schnell E, Sizemore M, Karimzadegan S, Chen L, Brecht DS, Nicoll RA. Direct interactions between PSD-95 and stargazin control synaptic AMPA receptor number. *Proc Natl Acad Sci USA* 2002; **99**: 13902–13907.
- 48 Beique JC, Lin DT, Kang MG, Aizawa H, Takamiya K, Huganir RL. Synapse-specific regulation of AMPA receptor function by PSD-95. *Proc Natl Acad Sci USA* 2006; **103**: 19535–19540.
- 49 Bats C, Groc L, Choquet D. The interaction between Stargazin and PSD-95 regulates AMPA receptor surface trafficking. *Neuron* 2007; **53**: 719–734.
- 50 Irwin SA, Patel B, Idupulapati M, Harris JB, Crisostomo RA, Larsen BP *et al*. Abnormal dendritic spine characteristics in the temporal and visual cortices of patients with fragile-X syndrome: a quantitative examination. *Am J Med Genet* 2001; **98**: 161–167.
- 51 Ehrlich I, Malinow R. Postsynaptic density 95 controls AMPA receptor incorporation during long-term potentiation and experience-driven synaptic plasticity. *J Neurosci* 2004; **24**: 916–927.
- 52 Ehrlich I, Klein M, Rumpel S, Malinow R. PSD-95 is required for activity-driven synapse stabilization. *Proc Natl Acad Sci USA* 2007; **104**: 4176–4181.
- 53 Mondin M, Labrousse V, Hosy E, Heine M, Tessier B, Levet F *et al*. Neurexin-neurologin adhesions capture surface-diffusing AMPA receptors through PSD-95 scaffolds. *J Neurosci* 2011; **31**: 13500–13515.
- 54 Aoto J, Martinelli DC, Malenka RC, Tabuchi K, Sudhof TC. Presynaptic neurexin-3 alternative splicing trans-synaptically controls postsynaptic AMPA receptor trafficking. *Cell* 2013; **154**: 75–88.
- 55 Shen PC, Xu DF, Liu JW, Li K, Lin M, Wang HT *et al*. TC10beta/CDC42 GTPase activating protein is required for the growth of cortical neuron dendrites. *Neuroscience* 2011; **199**: 589–597.
- 56 Tashiro A, Minden A, Yuste R. Regulation of dendritic spine morphology by the rho family of small GTPases: antagonistic roles of Rac and Rho. *Cereb Cortex* 2000; **10**: 927–938.
- 57 Vadodaria KC, Brakebusch C, Suter U, Jessberger S. Stage-specific functions of the small Rho GTPases Cdc42 and Rac1 for adult hippocampal neurogenesis. *J Neurosci* 2013; **33**: 1179–1189.
- 58 Kim IH, Wang H, Soderling SH, Yasuda R. Loss of Cdc42 leads to defects in synaptic plasticity and remote memory recall. *eLife* 2014; **3**: e02839.
- 59 Murakoshi H, Wang H, Yasuda R. Local, persistent activation of Rho GTPases during plasticity of single dendritic spines. *Nature* 2011; **472**: 100–104.

Supplementary Information accompanies the paper on the Molecular Psychiatry website (<http://www.nature.com/mp>)

Copyright of Molecular Psychiatry is the property of Nature Publishing Group and its content may not be copied or emailed to multiple sites or posted to a listserv without the copyright holder's express written permission. However, users may print, download, or email articles for individual use.